Hybridized Through-bond/Through-space Charge Transfer Enables Efficient Blue Emitters with Rec. 2020 Color Gamut

Xihao Yang,[1] Yongxu Hu,[1] Xiaoyu Guo, Jingsheng Miao, He Liu, Chuluo Yang*

Shenzhen Key Laboratory of New Information Display and Storage Materials, College of Materials Science and Engineering, Shenzhen University

Shenzhen 518055, P. R. China

E-mail: liuhe001@szu.edu.cn

1 There authors contribute equally to this work.

General information

All oxygen- and moisture-sensitive manipulations were carried out under an inert atmosphere. All the chemicals were purchased from commercial sources and used as received unless stated otherwise. Toluene was refluxed over Na and distilled under dry argon. Synthesized compounds were subject to purification by temperature gradient sublimation in high vacuum before used in subsequent studies. The 500 MHz ^{1}H and 125 MHz ^{13}C NMR spectra were recorded on a Bruker Ascend 500 spectrometer using $CDCl_3$ and DMSO-d_6 as solvent and tetramethylsilane (TMS) as an internal reference. Mass analyses were recorded by Bruker autoflex MALDI-TOF mass spectrometer. Photoluminescence (PL) spectra were recorded on a Hitachi F-4600 fluorescence spectrophotometer. Phosphorescence spectra of thin films were conducted at 77 K with 25 ms delay from excitation. Thermogravimetric analysis (TGA) was recorded on a TA Q50 instrument under nitrogen atmosphere at a heating rate of 10 ^{o}C/min from 200 ^{o}C to 800^{o}C. The temperature of degradation (T_d) was correlated to a 5% weight loss. Differential Scanning Calorimetry were carried out on a TA Q200. The glass transition temperature (T_g) was determined from the second heating scan at a heating rate of 10 ^{o}C min^{-1} from 50 to 300 ^{o}C. Cyclic voltammetry (CV) was carried out in nitrogen-purged dichloromethane (oxidation scan) at room temperature with a CHI voltametric analyzer. Tetrabutylammonium hexafluorophosphate (0.1 M) was used as the supporting electrolyte. The conventional three-electrode configuration consisted of a platinum working electrode, a platinum wire auxiliary electrode and an Ag wire pseudo-reference electrode with ferrocenium ferrocene (Fc^{+}/Fc) as the internal standard. Cyclic voltammograms were obtained at scan rate of 100 mV/s. Formal potentials were calculated as the average of cyclic voltametric anodic and cathodic peaks. The HOMO energy levels of the compounds were calculated according to the formula: -[4.8 + ($E_{1/2(ox/red)}$ - $E_{1/2(Fc/Fc+)}$)] eV. The onset potential was determined from the intersection of two tangents drawn at the rising and background current of the cyclic voltammogram. The solid-state absolute photoluminescence quantum yields (PLQYs)

were measured on a Hamamatsu UV-NIR absolute PL quantum yield spectrometer (C13534, Hamamatsu Photonics) equipped with a calibrated integrating sphere in the host of PPF (10 wt%). The PPF (10 wt%) films were spin-coated from chlorobenzene solutions. During the PLQY measurements, the integrating sphere was purged with pure and dry nitrogen to maintain an inert environment.

Computational Methods

All the density functional theory (DFT) calculations were carried out using Gaussian 09 package[1] on a Power Leader cluster. The ground-state geometry was fully optimized using DFT with B3LYP hybrid functional at the basis set level of 6-31G**. The excited-state properties were obtained by time-dependent density functional theory (TD-DFT) at the basis set level of B3LYP/6-31G**. In addition, the IFCT analysis were extracted by the Multiwfn code[2-4] and visualized using VMD.

Device Fabrication and Measurement

Glass substrates pre-coated with a 95-nm-thin layer of indium tin oxide (ITO) with a sheet resistance of 20 Ω per square were thoroughly cleaned for 50 minutes in ultrasonic bath of acetone, ethanol and isopropyl alcohol. Then, the cleaned glass substrates are dried by nitrogen purging. After that, in order to improving the hole injection ability of ITO, the substrates were treated by O_2 plasma for 10 minutes. Multilayer OLEDs were fabricated by the vacuum-deposition method. Organic layers were deposited by high-vacuum (~5 × 10^{-5} Pa) thermal evaporation onto a glass substrate pre-coated with an ITO layer. All organic layers were deposited sequentially. The thermal deposition rates for the organic materials, Liq and Al were 0.2~3.0, 0.5 and 3~5 Å s^{-1}, respectively. The active area of each device was 9 mm^2. The electroluminescence spectra, the current density-voltage characteristics and the current density-voltage-luminance curves characterizations of the OLEDs were carried out with a Photo Research Spectra Scan PR-745 Spectroradiometer and a Keithley 2450

Source Meter and they are recorded simultaneously. All measurements were done at room temperature under ambient conditions.

Analysis of rate constants

Time-resolved transient photoluminescence decay measurements were utilized to research the delayed fluorescence phenomenon of the molecule in doped films (20 wt% in PPF), Rate constants of different kinetic processes were calculated following the equations (S1) - (S6) below:[5,6]

$$k_p = \frac{1}{\tau_p} \quad (1)$$

$$k_d = \frac{1}{\tau_d} \quad (2)$$

$$k_{r,s} = \Phi_p k_p + \Phi_d k_d \quad (3)$$

$$k_{RISC} \approx \frac{k_p k_d \Phi}{k_{r,s}} \quad (4)$$

$$k_{ISC} \approx \frac{k_p k_d \Phi_d}{k_{RISC} \Phi_p} \quad (5)$$

Where $k_{r,s}$, k_{nr}, k_{ISC}, k_{RISC} represent the rate constant of singlet radiative decay, non-radiative decay, intersystem crossing and reverse intersystem crossing, respectively; Φ, Φ_P, Φ_d, τ_p and τ_d represent total PLQY, quantum yield of the prompt component, quantum yield of the delayed component, lifetimes of the prompt and delayed components, respectively.

In this study, Φp and Φd were determined by using the total PLQY and the integrated intensity ratio between prompt and delayed components which was calculated from transient photoluminescence measurements. The intensity ratio between prompt (rp) and delayed (rd) components were determined using two fluorescent lifetimes (τp, τd) and fitting parameter (Ap, Ad) as follow.

$$I(t) = A_p e^{-\frac{t}{\tau_p}} + A_d e^{-\frac{t}{\tau_d}} \quad (6)$$

$$r_p = \frac{A_p\tau_p}{A_p\tau_p + A_d\tau_d} \quad (7)$$

$$r_d = \frac{A_d\tau_d}{A_p\tau_p + A_d\tau_d} \quad (8)$$

Then, the prompt PLQY (Φ_p) and delayed PLQY (Φ_d) were determined using intensity ratio (rp, rd) and total PLQY.

$$\Phi = \Phi_p + \Phi_d \quad (9)$$

$$\Phi_p = r_p\Phi \quad (10)$$

$$\Phi_d = r_d\Phi \quad (11)$$

Analysis of efficiency roll-off

The TTA mode simulation can be described as follows:[7]

$$\frac{\eta_{ext}^{TT}(J)}{\eta_0} = \frac{J_0}{4J}\left(\sqrt{1 + 8\frac{J}{J_0}} - 1\right) \quad (12)$$

where η, η_0, and J_0 represent the EQE in the presence of TTA, initial EQE in the absence of TTA (at very low current densities, rendering the TTA quenching negligible), and the current density at the half-maximum of the EQE, respectively.

The SPA model, which can be expressed by Equation: [7]

$$\frac{\eta_{ext}^{SP}(J)}{\eta_0} = \frac{1}{1 + \left(\frac{J}{J_0}\right)^{\frac{1}{l+1}}} \quad (13)$$

where η_{ext}^{SP} is the EQE in the presence of SPA and l is the fitting parameter. According to the previous work, l needs to be an integer greater than 1 to make this equation reasonable, and here $l = 2$ after fitting.

The STA mode simulation can be described as follows:[8]

$$\frac{\eta_{ext}^{STA}(J)}{\eta_0} = \frac{1}{1+\frac{J}{J_0}} \qquad (14)$$

where η, η_0, and J_0 represent the EQE in the presence of STA, initial EQE in the absence of STA (at very low current densities, rendering the STA quenching negligible), and the current density at the half-maximum of the EQE, respectively.

Reference

1. M. J. Frisch, G. W. Trucks, H. B. Schlegel, G. E. Scuseria, M. A. Robb, J. R. Cheeseman, G. Scalmani, V. Barone, B. Mennucci, G. A. Petersson, H. Nakatsuji, M. Caricato, X. Li, H. P. Hratchian, A. F. Izmaylov, J. Bloino, G. Zheng, J. L. Sonnenberg, M. Hada, M. Ehara, K. Toyota, R. Fukuda, J. Hasegawa, M. Ishida, T. Nakajima, Y. Honda, O. Kitao, H. Nakai, T. Vreven, J. A. Montgomery Jr, J. E. Peralta, F. Ogliaro, M. Bearpark, J. J. Heyd, E. Brothers, K. N. Kudin, V. N. Staroverov, R. Kobayashi, J. Normand, K. Raghavachari, A. Rendell, J. C. Burant, S. S. Iyengar, J. Tomasi, M. Cossi, N. Rega, J. M. Millam, M. Klene, J. E. Knox, J. B. Cross, V. Bakken, C. Adamo, J. Jaramillo, R. Gomperts, R. E. Stratmann, O. Yazyev, A. J. Austin, R. Cammi, C. Pomelli, J. W. Ochterski, R. L. Martin, K. Morokuma, V. G. Zakrzewski, G. A. Voth, P. Salvador, J. J. Dannenberg, S. Dapprich, A. D. Daniels, Ö . Farkas, J. B. Foresman, J. V. Ortiz, J. Cioslowski, D. J. Fox, Revision D.01 ed., Gaussian, Inc., Wallingford CT, **2009**

2. E. R. Johnson, S. Keinan, P. Mori-Sánchez, J. Contreras-García, A. J. Cohen, W. Yang, *J. Am. Chem. Soc.* **2010**, *132*, 6498-6506.

3. Z. Yang, Z. Mao, C. Xu, X. Chen, J. Zhao, Z. Yang, Y. Zhang, W. Wu, S. Jiao, Y. Liu, M. P. Aldred, Z. Chi*, Chem. Sci.* **2019**, *10*, 8129-8134.

4. T. Lu, F. Chen, *J. Comput. Chem.* **2012**, *33*, 580-592

5. K.-C. Pan, S.-W. Li, Y.-Y. Ho, Y.-J. Shiu, W.-L. Tsai, M. Jiao, W.-K. Lee, C.-C. Wu, C.-L. Chung, T. Chatterjee, Y. S.-Li, K.-T. Wong, H.-C. Hu, C.-C. Chen, M.-T. Lee. *Adv. Funct. Mater.* **2016**, 26, 7560-7571

6. L. Gan, K. Gao, X. Cai, D. Chen. S.-J. Su. *J. Phys. Chem. Lett.* **2018**, 9, 4725-4731.

7. S. Reineke, K. Walzer, K. Leo, Triplet-exciton quenching in organic phosphorescent light-emitting diodes with Ir-based emitters. *Phys. Rev. B.* **2007,** *75*, 125328.

8. B. van der Zee, Y. Li, G. J. A. H. Wetzelaer, P. W. M. Blom, "Origin of the efficiency roll-off in single-layer organic light-emitting diodes based on thermally activated delayed fluorescence," *Adv. Opt. Mater.* **2021**, *9*, 2100249.

Synthesis and characterization

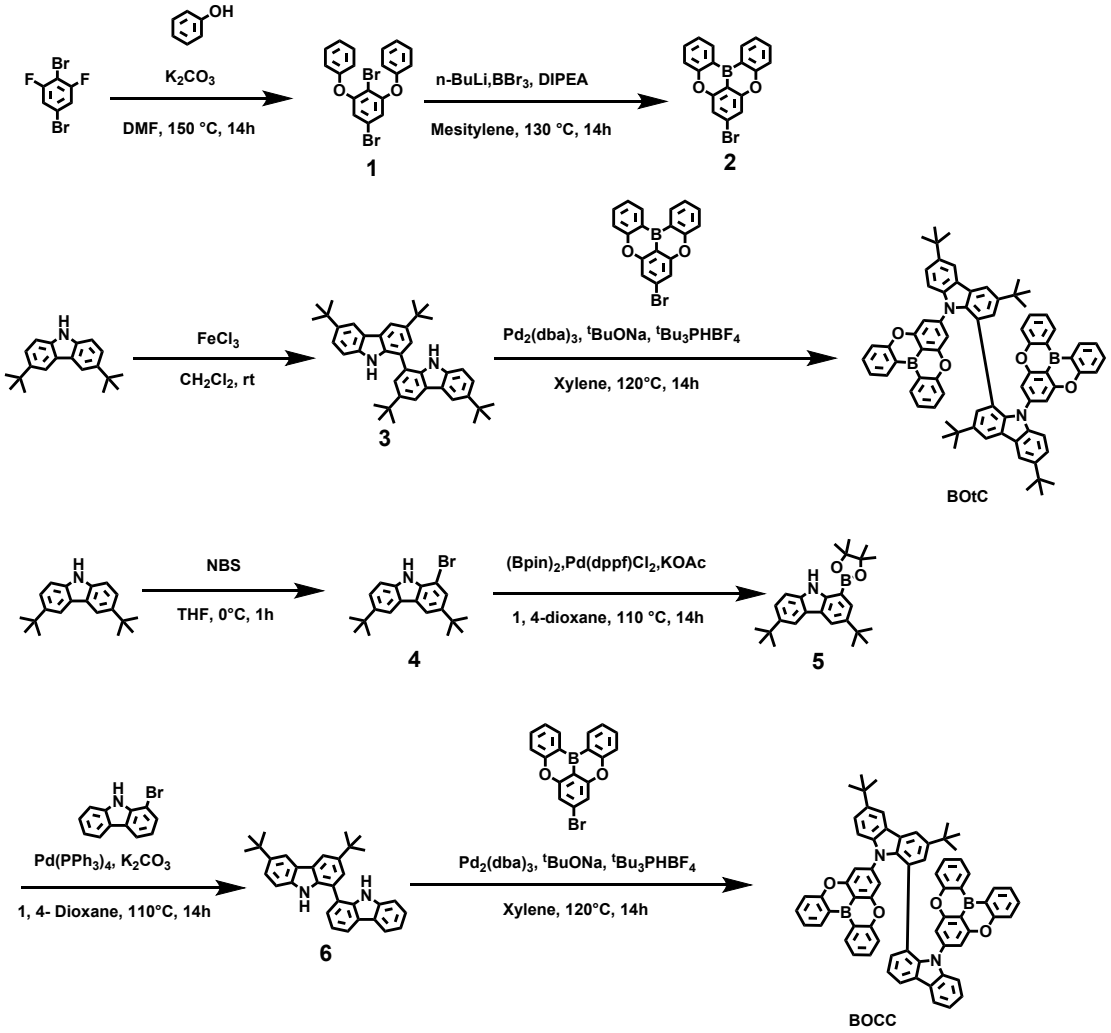

Scheme S1. The synthetic route of 2tCZBO, 2CZBO and tCZCZBO.

((2,5-dibromo-1,3-phenylene)bis(oxy))dibenzene (1)

2,5-dibromo-1,3-difluorobenzene (8 g, 25.5 mmol), phenol (11 g, 116.9 mmol), K_2CO_3 (20 g, 144.8 mmol) and super-dry *N*,*N*-Dimethylformamide (50 mL) were added into a 100 mL branch bottle under N_2 atmosphere. The mixture was heated to 150 °C and stirred for 16 h. After cooling to room temperature, the mixture was poured into water and stirred for 10 minutes. The mixture was filtered and the solid was washed by water and ethanol to give the intermediate 1 as a pink solid (11 g, Yield: 89%).^{1}H NMR (500 MHz, Chloroform-*d*) δ 7.42 – 7.38 (t, *J* = 7.5 Hz, 4H), 7.20 (t, *J* = 7 Hz, 2H), 7.06 (d, *J* = 7.5 Hz, 4H), 6.75 (s, 2H).

7-bromo-5,9-dioxa-13b-boranaphtho[3,2,1-de]anthracene (2)

1.2 M *n*-BuLi in hexane (5.3 mL, 8.5 mmol) was added into a solution of intermediate **1** (3 g, 6.9 mmol) in 40 mL super-dry mesitylene under N_2 atmosphere at 0 °C. After stirring for 15 min, the mixture was stirred at room temperature for 1 h. When the mixture cooling down, boron tribromide (1.4 mL, 14.5 mmol) was added at 0 ℃, then the reaction was stirred at room temperature for 1 h. After *N*,*N*-diisopropylethylamine (3 mL, 18 mmol) was added at 0 ℃, the reaction was heated up to 130 ℃ and stirred for 14 h. After cooling to room temperature, the mixture was poured into ethanol and stirred for 10 min. The mixture was filtered to give the product as a colorless solid (1.5 g, Yield: 54%).^{1}H NMR (500 MHz, Chloroform-*d*) δ 8.70 (d, *J* = 7.7 Hz, 2H), 7.75 (t, *J* = 7.8 Hz, 2H), 7.56 (d, *J* = 9.5 Hz, 2H), 7.44 (s, 2H), 7.43 (t, *J* = 7.9 Hz, 2H).

3,3',6,6'-Tetra-tert-butyl-1,1'-bicarbazole (3)

To a solution of 3,6-di-tert-butylcarbazole (1.00 g, 3.58 mmol) in CH_2Cl_2 (100 mL) was added dropwise a solution of $FeCl_3$ (1.16 g, 7.16mmol) in CH_2Cl_2 (100 mL) at room temperature. After stirring for 30 min, the reaction was quenched by addition of MeOH (20 ml). The reaction mixture was added to water (100 mL) and extracted with CH_2Cl_2 (50 mL × 3). The organic layer was dried over Na_2SO_4, filtered, and concentrated under reduced pressure. Purification via column chromatography on silica gel (200-300 mesh, petroleum ether/dichloromethane = 9:1 v/v) afford a colorless solid (360 mg, Yield: 36%). ^{1}H NMR (500 MHz, DMSO-d_6) δ 10.37 (s, 2H), 8.26 (s, 2H), 8.21 (s, 2H), 7.51 (s, 2H), 7.41 (d, *J* = 10.5 Hz, 2H), 7.32 (d, *J* = 8.5 Hz, 2H), 1.48 (s, 18H), 1.42 (s, 18H).

9,9'-di(5,9-dioxa-13b-boranaphtho[3,2,1-de]anthracen-7-yl)-3,3',6,6'-tetra-tert-butyl-9H,9'H-1,1'-bicarbazole (BOtC)

2 (470 mg, 1.35 mmol), 3 (300 mg, 0.53 mmol) and xylene (15 mL) were added into a 100 mL branch bottle under N_2 atmosphere. After the mixture was degassed for 10 minutes, tris(dibenzylideneacetone)dipalladium (60 mg, 0.06 mmol), sodium tert-butanol (210 mg, 2.18 mmol) and tri-tert-butylphosphine tetrafluoroborate (60 mg, 0.20 mmol) were added into the bottle under the N_2 atmosphere. The mixture was stirred at 120 °C for 14 h. After cooling and vacuum filtrating, the filtrate was evaporated under reduced pressure. Purification via column chromatography on silica gel (200-300 mesh, petroleum ether/dichloromethane = 9:1 v/v) afford a colorless solid (270 mg, Yield: 32%). ^{1}H NMR (500 MHz, Methylene Chloride-d_2) δ 8.68 (d, J = 7.7 Hz, 4H), 7.68 (s, 4H), 7.58 (d, J = 1.9 Hz, 2H), 7.51 (d, J = 1.9 Hz, 2H), 7.46 – 7.31 (m, 10H), 7.30 – 7.15 (m, 4H), 7.09 (s, 2H), 6.34 (s, 2H), 1.26 (s, 18H), 1.17 (s, 18H). ^{13}C NMR (125 MHz, $CDCl_3$) δ 160.3, 156.2, 143.4, 143.2, 143.1, 134.0, 136.3, 134.4, 133.3, 125.4, 124.6, 124.0, 123.5, 123.4, 122.6, 118.6, 115.5, 114.6, 112.7 109.4, 34.5, 34.4, 31.8, 31.7. MALDI-TOF: calcd for $C_{76}H_{66}B_2N_2O_4$ m/z 1092.99; found 1092.752

1-bromo-3,6-di-tert-butyl-9H-carbazole (4)

To a solution of 3,6-di-tert-butyl-9H-carbazole (1 g, 3.57 mmol) in $CHCl_3$ (10 mL) was added N-bromosuccinimide (636 mg, 3.57 mmol) at 0 °C, and the mixture was stirred at rt for 2 h in the dark. After vacuum filtrating, the filtrate was evaporated under reduced pressure. Purification via column chromatography on silica gel (200-300 mesh, petroleum ether/dichloromethane = 9:1 v/v) afford a colorless solid (1.24 g, Yield: 95%). ^{1}H NMR (500 MHz, Chloroform-*d*) δ 8.10 (s, 1H), 8.07 (s, 1H), 8.04 (s, 1H), 7.62 (s, 1H), 7.54 (d, J = 8.6 Hz, 1H), 7.42 (d, J = 8.5 Hz, 1H), 1.49 – 1.46 (m, 18H).

3,6-di-tert-butyl-1-(4,4,5,5-tetramethyl-1,3,2-dioxaborolan-2-yl)-9H-carbazole (5)

5 (600 mg, 1.67 mmol), 4,4,4',4',5,5,5',5'-octamethyl-2,2'-bi(1,3,2-dioxaborolane) (1.7 g, 6.69 mmol), [1,1'-Bis(diphenylphosphino)ferrocene]dichloropalladium(II) (104 mg,

0.13 mmol), potassium acetate (328 mg, 3.34 mmol), super-dry 1,4-dioxane (15 mL) were added into a 100 mL branch bottle under N_2 atmosphere. The mixture was stirred at 110 °C for 14 h. After cooling to room temperature, the filtrate was evaporated under reduced pressure. Purification via column chromatography on silica gel (200-300 mesh, petroleum ether/dichloromethane = 8:1 v/v) afford a colorless solid (330 mg, Yield: 48%). ^{1}H NMR (500 MHz, Chloroform-*d*) δ 8.95 (s, 1H), 8.21 (d, *J* = 2.0 Hz, 1H), 8.07 (s, 1H), 7.88 (d, *J* = 2.0 Hz, 1H), 7.46 (dd, *J* = 8.5, 1.9 Hz, 1H), 7.39 (d, *J* = 8.4 Hz, 1H), 1.47 (s, 9H), 1.45 (s, 9H), 1.43 (s, 12H).

3,6-di-tert-butyl-9H,9'H-1,1'-bicarbazole (6)

6 (300 mg, 0.74 mmol), 1-Bromo-9H-carbazole（200 mg, 0.81 mmol）, tetrakis(triphenylphosphine)palladium (43 mg, 0.03 mmol), Potassium carbonate (409 mg, 2.96 mmol), super-dry 1,4-dioxane (15 mL) were added into a 100 mL branch bottle under N_2 atmosphere. The mixture was stirred at 110 °C for 14 h. After cooling to room temperature, the filtrate was evaporated under reduced pressure. Purification via column chromatography on silica gel (200-300 mesh, petroleum ether/dichloromethane = 8:1 v/v) afford a colorless solid (210 mg, Yield: 64%). ^{1}H NMR (500 MHz, DMSO-d_6) δ 10.66 (s, 1H), 10.47 (s, 1H), 8.27 (s, 1H), 8.23 – 8.17 (m, 3H), 7.51 (d, *J* = 8.2 Hz, 2H), 7.44 (d, *J* = 7.5 Hz, 1H), 7.44 (d, *J* = 8.4 Hz, 1H), 7.37 – 7.31 (m, 3H), 7.17 (t, *J* = 7.5 Hz, 1H), 1.48 (s, 9H), 1.42 (s, 9H).

9,9'-di(5,9-dioxa-13b-boranaphtho[3,2,1-de]anthracen-7-yl)-3,6-di-tert-butyl-9H,9'H-1,1'-bicarbazole (BOCC)

2 (376 mg, 1.07 mmol), 7 (200 mg, 0.45 mmol) and xylene (15 mL) were added into a 100 mL branch bottle under N_2 atmosphere. After the mixture was degassed for 10 minutes, tris(dibenzylideneacetone)dipalladium (42 mg, 0.04 mmol), sodium tert-butanol (174 mg, 1.81 mmol) and tri-tert-butylphosphine tetrafluoroborate (40 mg, 0.14 mmol) were added into the bottle under the N_2 atmosphere. The mixture was stirred at 120 °C for 14 h. After cooling and vacuum filtrating, the filtrate was evaporated under reduced pressure. Purification via column chromatography on silica gel (200-300 mesh,

petroleum ether/dichloromethane = 9:1 v/v) afford a colorless solid (220 mg, Yield: 50%).^{1}H NMR (500 MHz, Methylene Chloride-d_2) δ 8.70 (d, J = 7.7 Hz, 4H), 7.75 – 7.65 (m, 4H), 7.61 – 7.56 (m, 2H), 7.50 (t, J = 1.3 Hz, 1H), 7.47 – 7.32 (m, 10H), 7.29 – 7.15 (m, 5H), 7.03 (t, J = 7.5 Hz, 3H), 6.78 (t, J = 7.3 Hz, 1H), 6.35 – 6.18 (m, 2H), 1.23 (s, 9H), 1.18 (s, 9H). ^{13}C NMR (126 MHz, $CDCl_3$) δ 160.5, 160.3, 156.0, 143.4, 143.2, 142.5, 142.2, 141.1, 139.3, 137.3, 135.8, 134.4, 133.3, 127.8, 125.8, 125.1, 125.0, 124.6, 124.5, 123.6, 123.4, 123.3, 123.3, 122.6, 120.3, 120.3, 119.4, 118.6, 118.3, 115.4, 114.6, 112.8, 109.7, 109.2, 107.4, 106.2, 34.5, 34.4, 31.7.

Supplymantery Figures

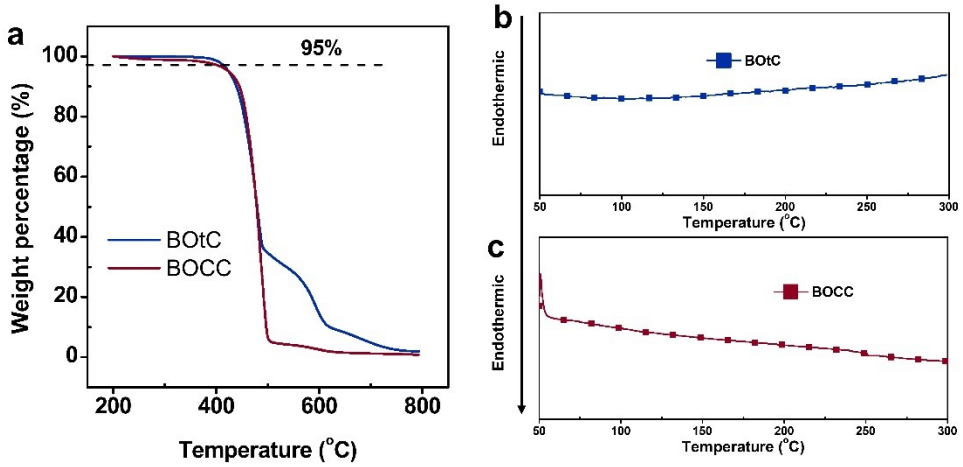

Figure S1. Thermal properties of BOtC and BOCC. a) TGA profiles, b, c) DSC curves.

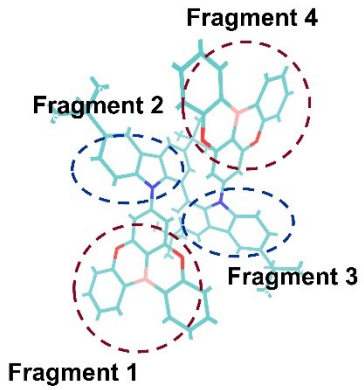

BOtC-S1	1	2	3	4
1	0.01433	0.00045	0.00044	0.01424
2	0.22891	0.00713	0.00710	0.22749
3	0.22883	0.00712	0.00710	0.22740
4	0.01433	0.00045	0.00044	0.01424

BOtC-T1	1	2	3	4
1	0.13507	0.00423	0.00423	0.13463
2	0.10772	0.00338	0.00337	0.10737
3	0.10768	0.00338	0.00337	0.10733
4	0.13510	0.0.00423	0.00423	0.13466

Figure S2. Detailed IFCT analysis of BOtC.

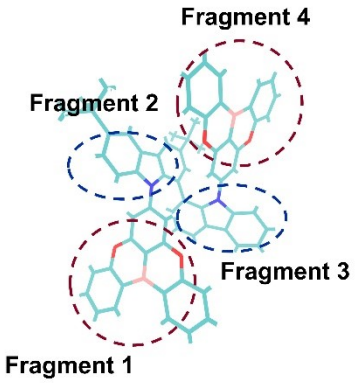

BOCC-S1	1	2	3	4
1	0.01294	0.00044	0.00064	0.02585
2	0.27375	0.00923	0.01356	0.54692
3	0.03174	0.00107	0.00157	0.06342
4	0.00612	0.00021	0.00030	0.01222

BOCC-T1	1	2	3	4
1	0.00135	0.00018	0.00059	0.02614
2	0.01463	0.00191	0.00640	0.28275
3	0.00156	0.00020	0.00068	0.03020
4	0.03031	0.00020	0.01326	0.58589

Figure S3. Detailed IFCT analysis of BOCC.

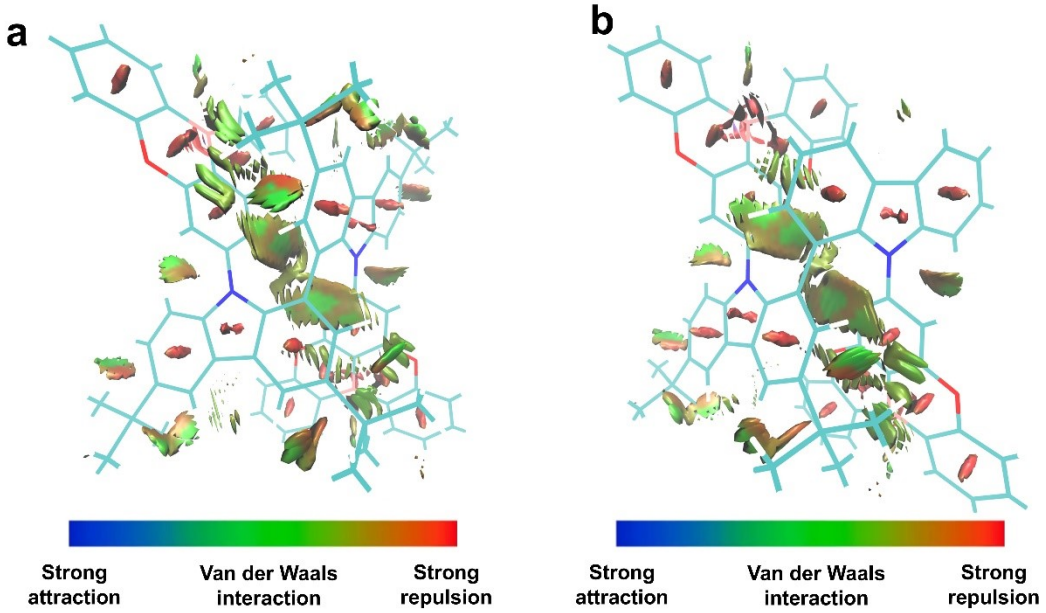

Figure S4. RDG analysis of a) BOtC and b) BOCC.

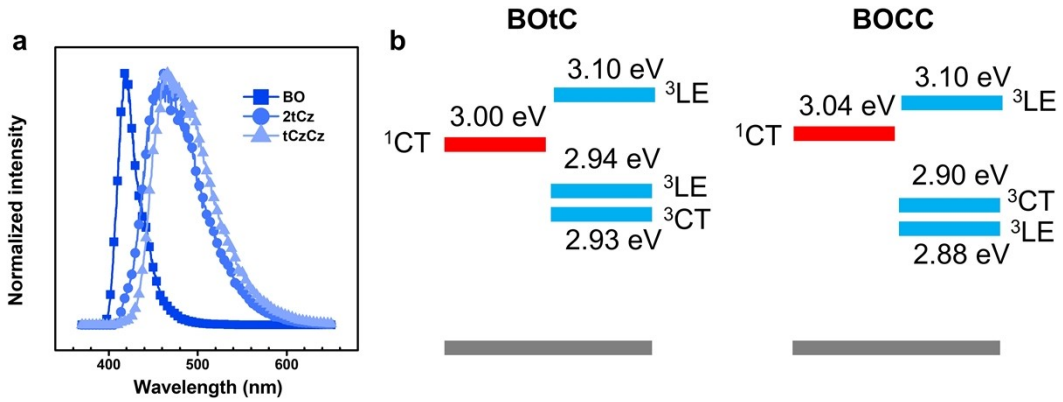

Figure S5. a) Phosphorescent spectra of the donor and acceptor motifs, b) energy alignments of BOtC and BOCC.

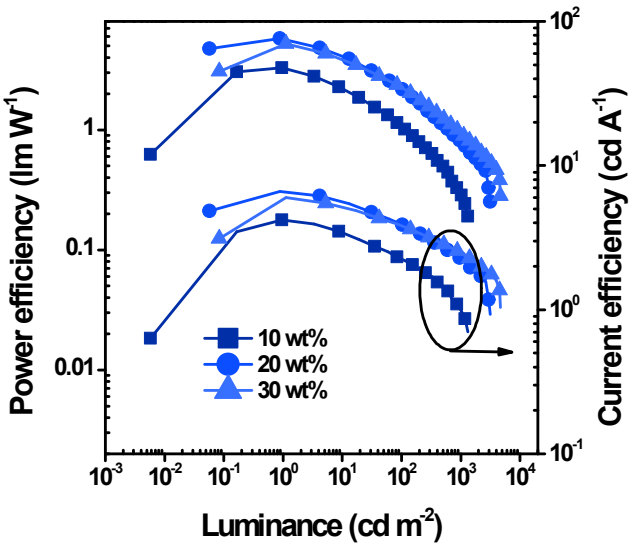

Figure S6. EL performance of BOtC under different doping levels.

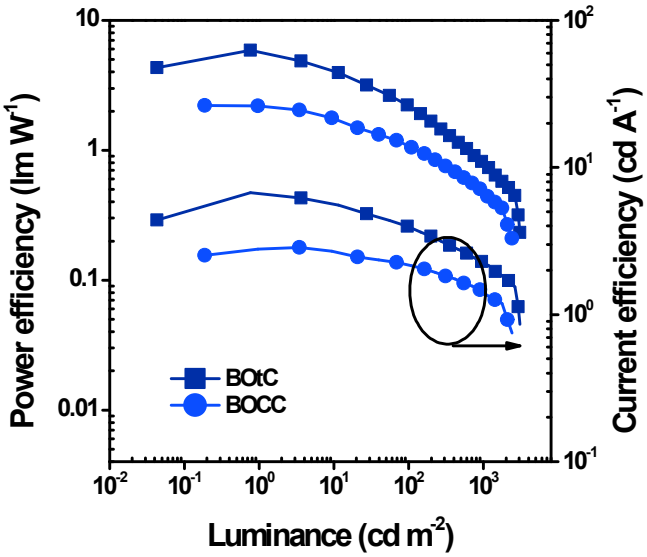

Figure S7. EL performance of BOtC and BOCC.

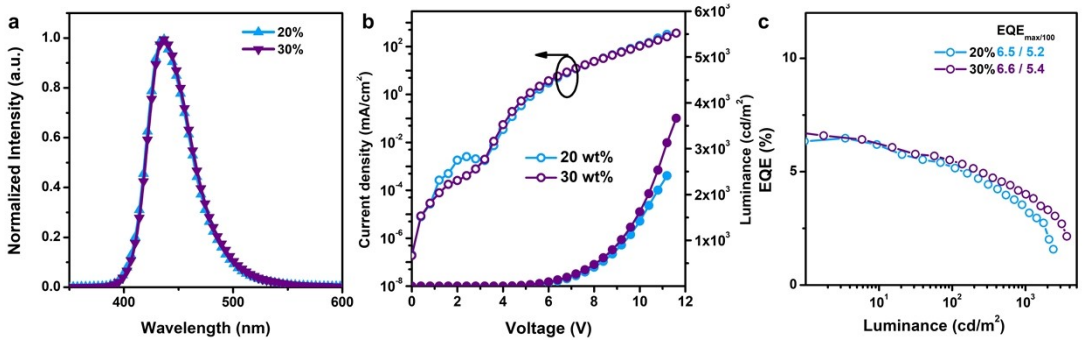

Figure S8. EL performance of BOCC under different doping concentration. a) EL spectra, b) *J*-*V*-*L* curves, c) EQE-*J* profiles.

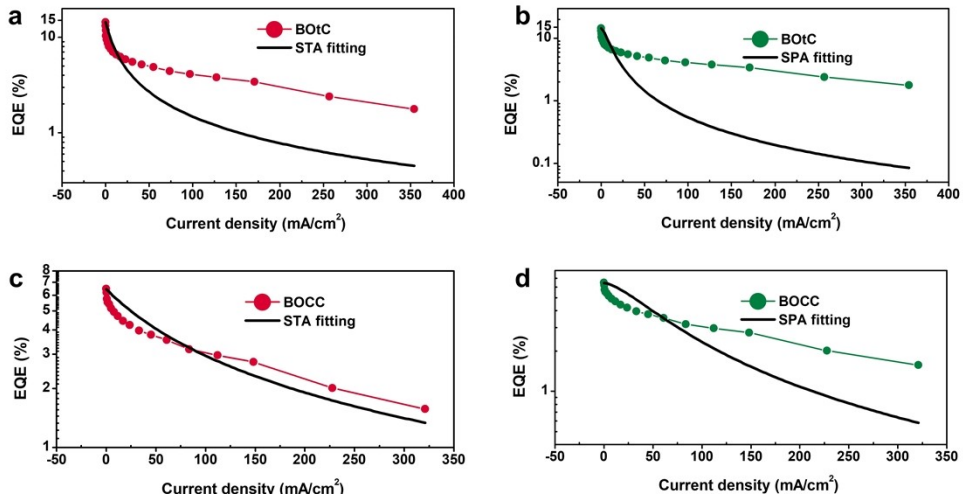

Figure S9. Fitting of the EQE-*J* of BOtC and BOCC profiles using STA and SPA models.

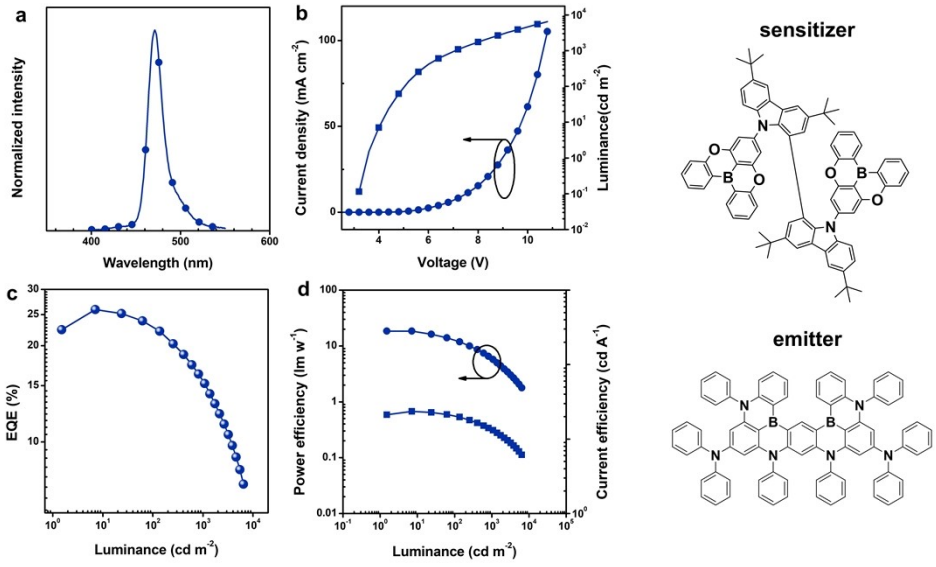

Figure S10. EL performance of sensitized devices. a) EL spectra, b) *J*-*V*-*L* curves, c) EQE-*L* profiles, d) PE-*L* and CE-*L* behaviors.

Supplymantery Table

Table 1. Crystal data and structure refinement for BOtC.

Empirical formula	$C_{76}H_{66}B_2N_2O_4$
Formula weight	1092.92
Temperature/K	100.00
Crystal system	triclinic
Space group	P-1
a/Å	11.4412(3)
b/Å	13.8790(3)
c/Å	22.1353(5)
α/°	80.5370(10)
β/°	79.1210(10)
γ/°	75.2690(10)
Volume/Å^3	3313.12(14)
Z	2
ρ_{calc}g/cm^3	1.096
μ/mm^{-1}	0.514
F(000)	1156.0
Crystal size/mm^3	0.4 × 0.2 × 0.2
Radiation	CuKα (λ = 1.54178)
2Θ range for data collection/°	7.36 to 136.606
Index ranges	-13 ≤ h ≤ 13, -16 ≤ k ≤ 16, -26 ≤ l ≤ 26
Reflections collected	74145
Independent reflections	12083 [R_{int} = 0.0448, R_{sigma} = 0.0283]
Data/restraints/parameters	12083/0/770
Goodness-of-fit on F^2	1.041
Final R indexes [I>=2σ (I)]	R_1 = 0.0402, wR_2 = 0.0981
Final R indexes [all data]	R_1 = 0.0436, wR_2 = 0.1003
Largest diff. peak/hole / e Å^{-3}	0.26/-0.23

Table S2. EL performance of sensitized devices based on BOtC.

EML	λ (nm)	V_{on} (V)	*L* (cd/m^2)	EQE (%)	CE (cd/A)	CIE (x, y)
20%BOtC:1%v-DABNA	470	3.6	6454	25.9/20.5/13.4	23.5	0.120, 0.117

NMR spectra

^{1}H NMR spectra of **1** ($CDCl_3$)

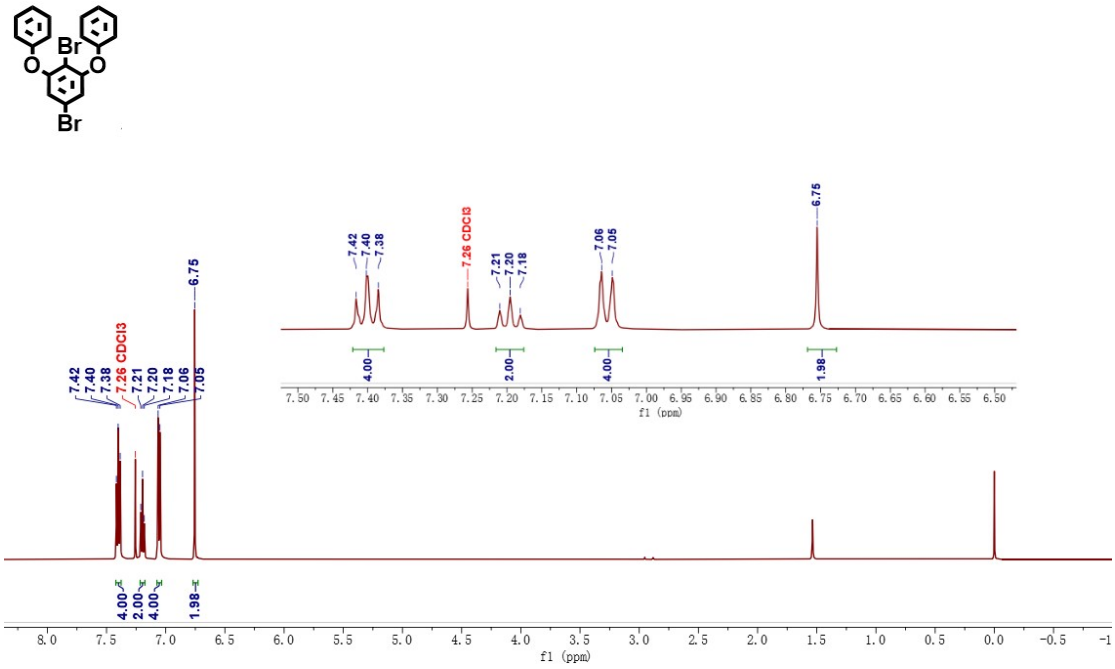

^{1}H NMR spectra of **2** ($CDCl_3$)

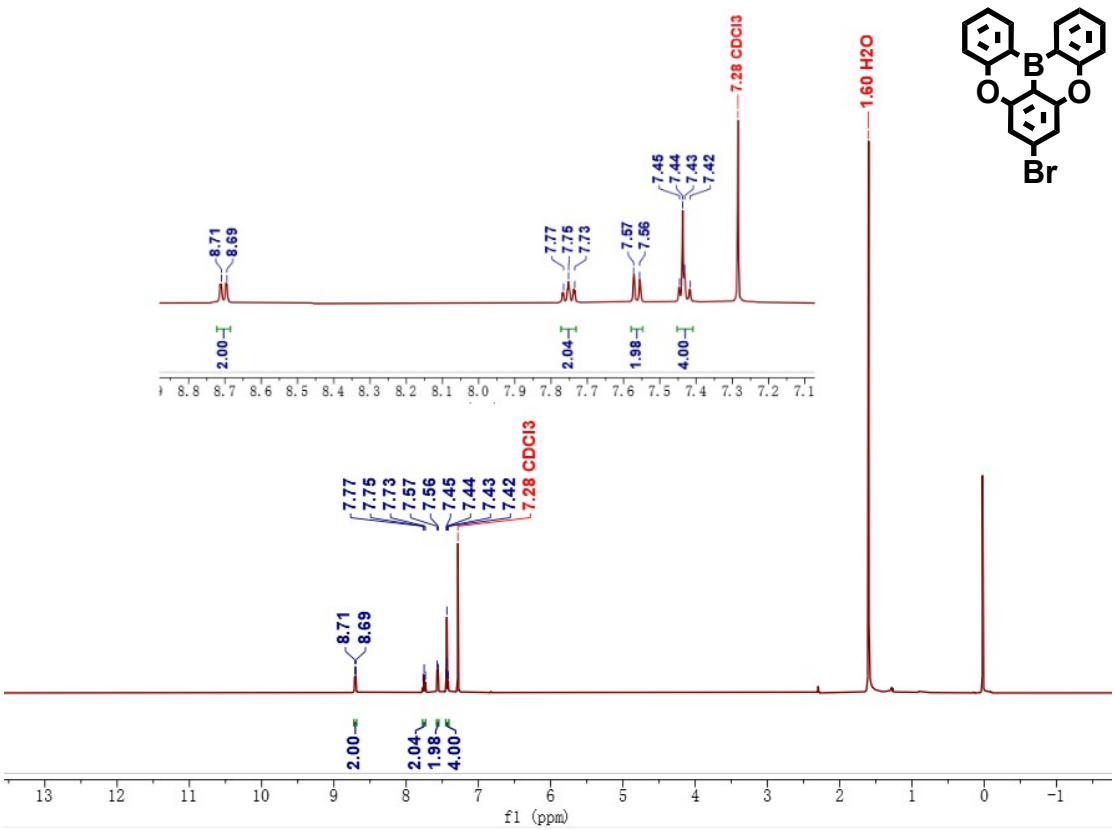

^{1}H NMR spectra of **3** ($CDCl_3$)

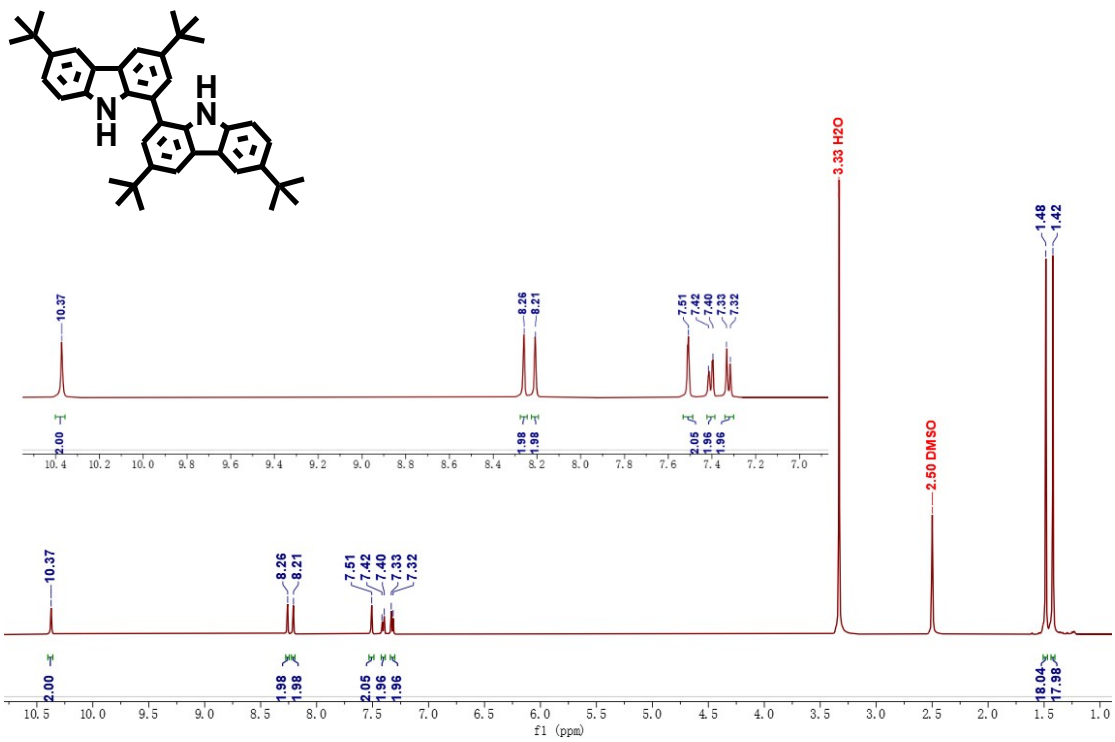

^{1}H NMR spectra of **2tCZBO** (CD_2Cl_2)

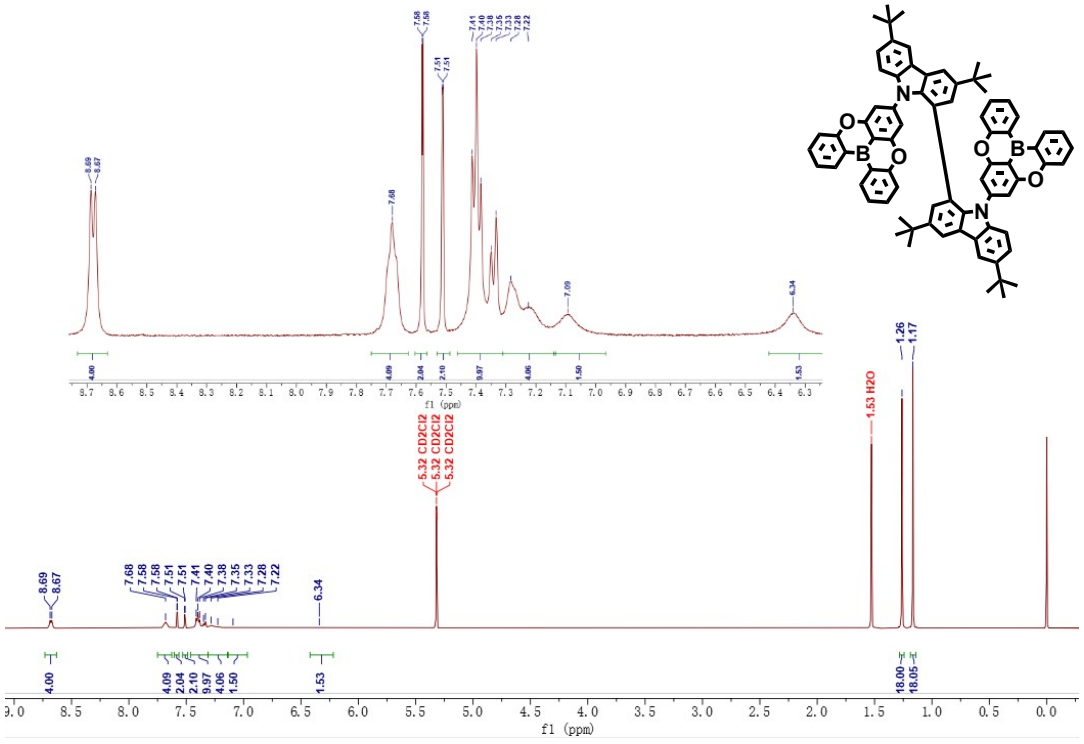

^{13}C NMR spectra of **2tCZBO** ($CDCl_3$)

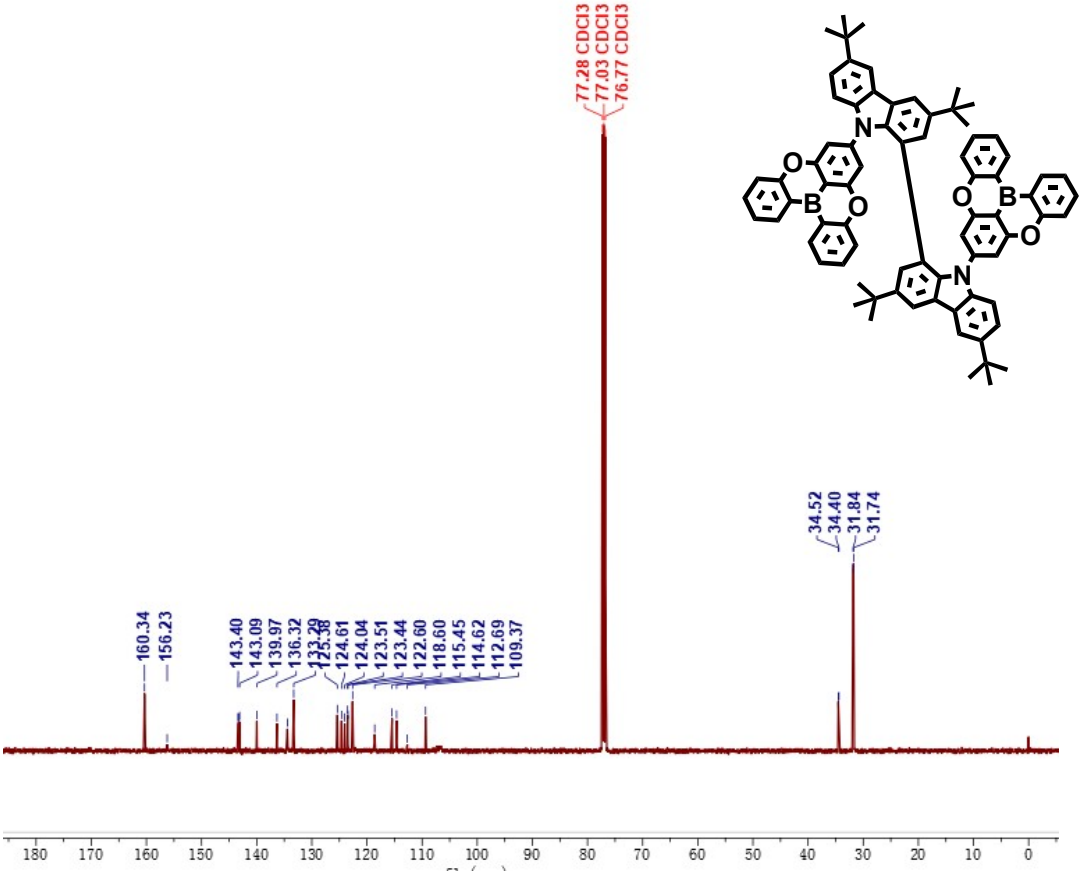

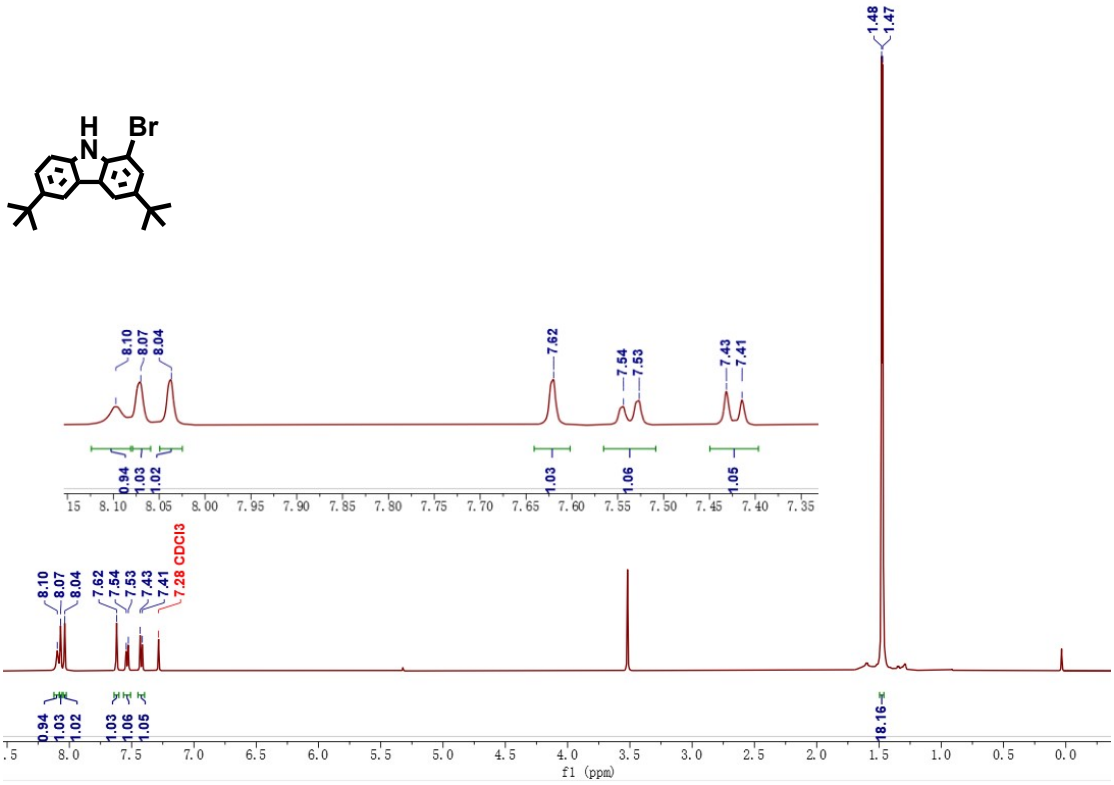

^{1}H NMR spectra of **6** ($CDCl_3$)

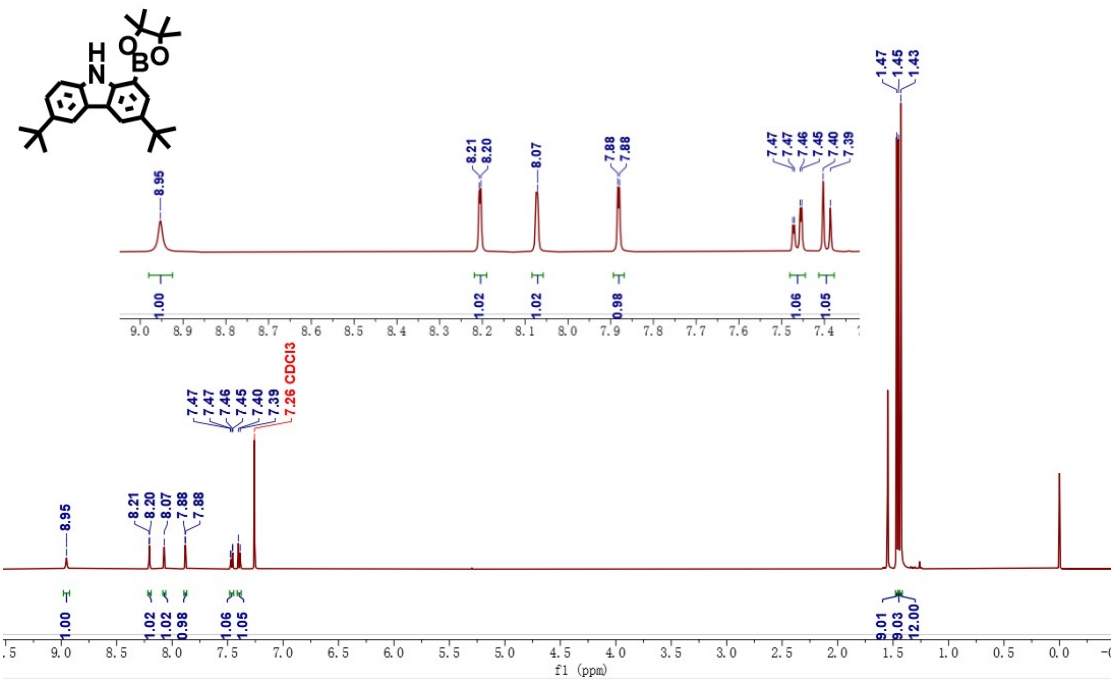

^{1}H NMR spectra of **7** (DMSO-d_6)

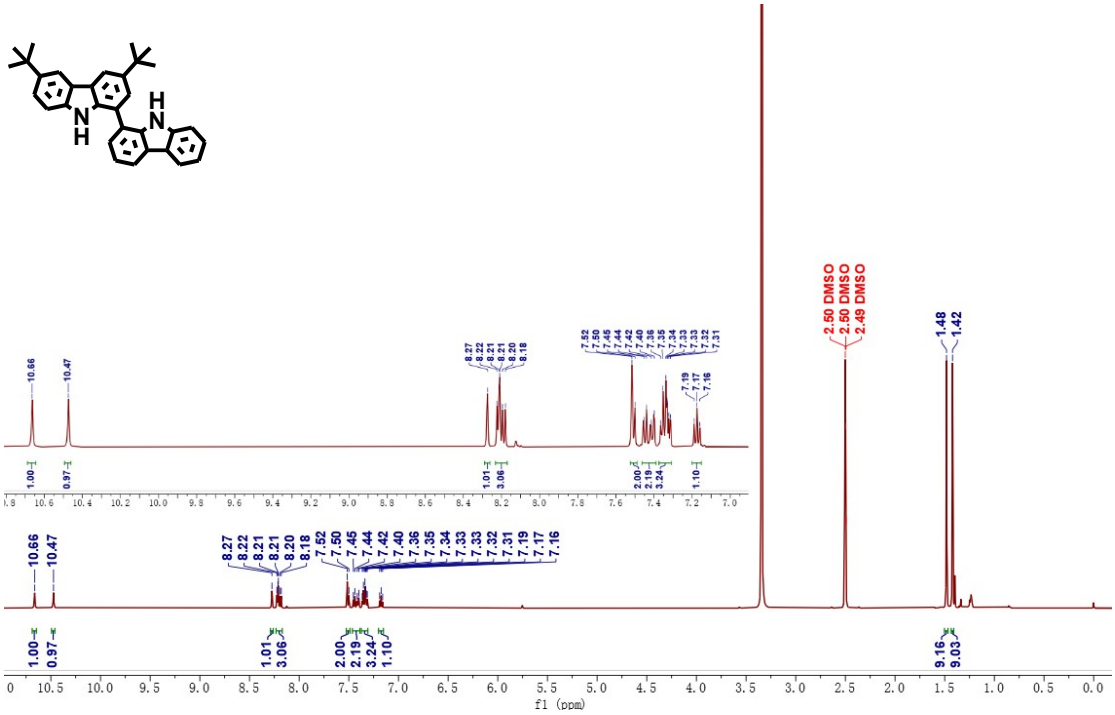

^{1}H NMR spectra of **tCZCZBO** (CD_2Cl_2)

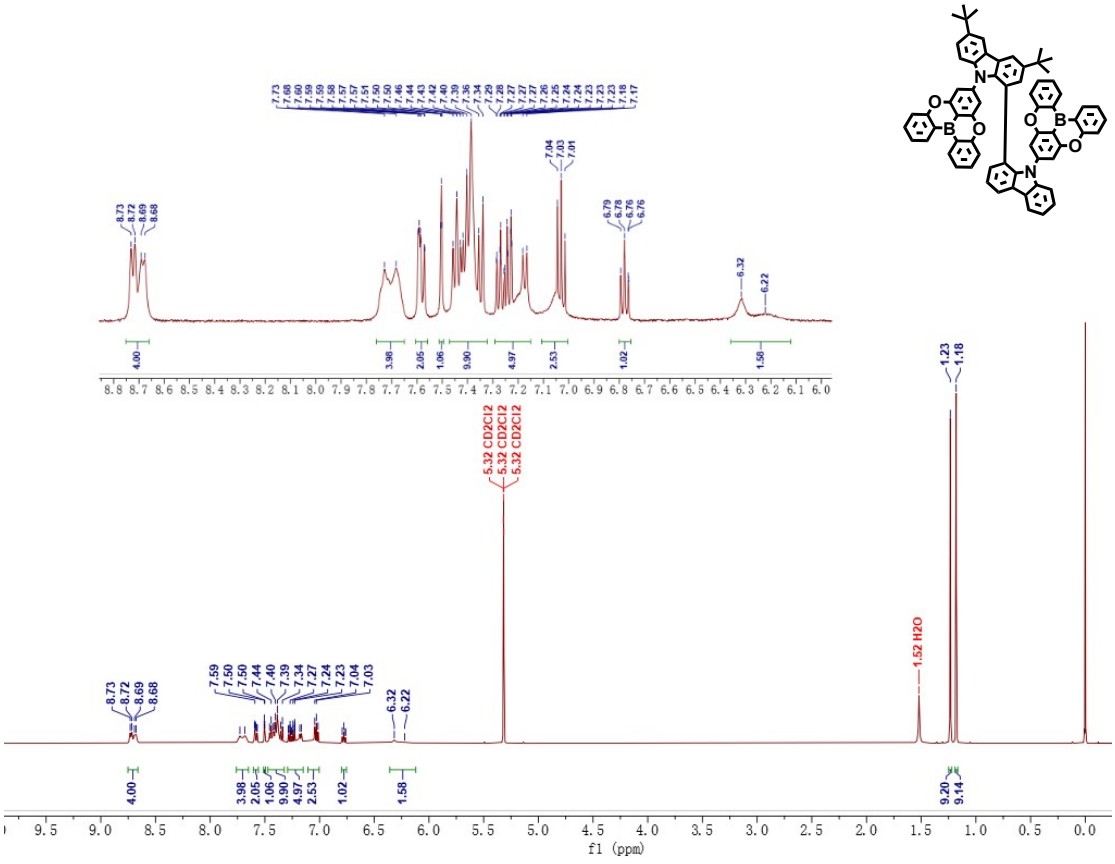

^{13}C NMR spectra of **2tCZBO** ($CDCl_3$)

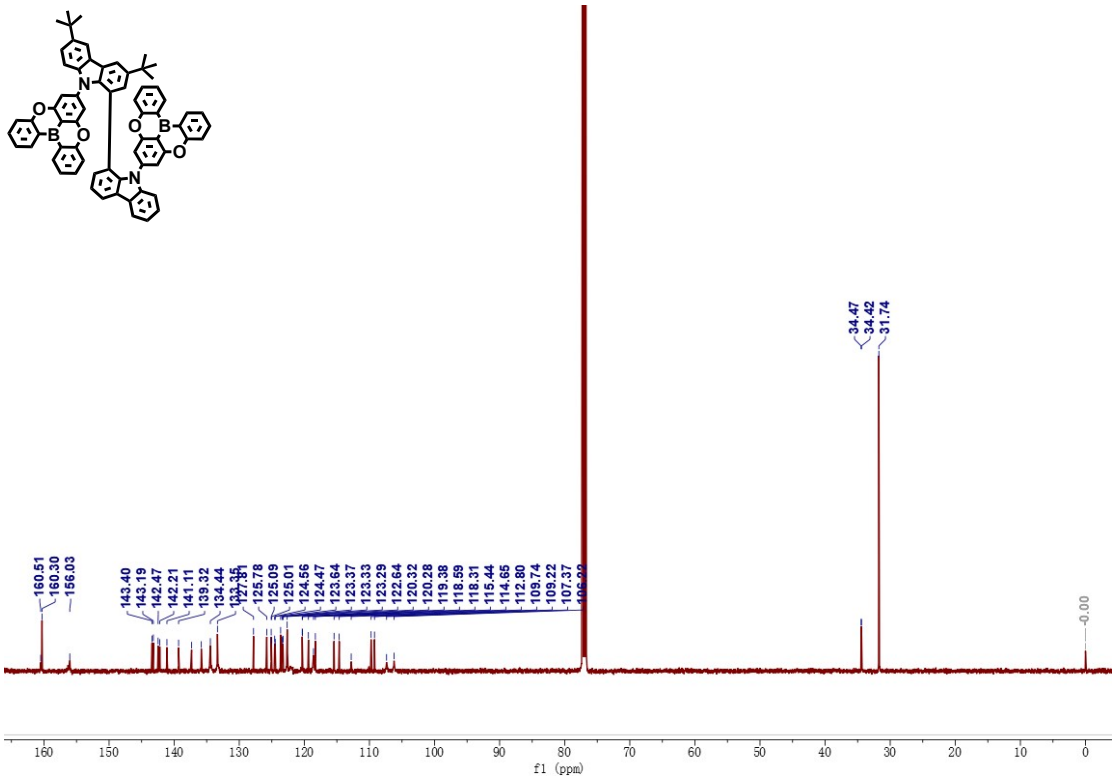
160.51
160.30
156.03
143.40
143.19
142.47
142.21
141.11
139.32
134.44
133.35
127.81
125.78
125.09
125.01
124.56
124.47
123.64
123.37
123.33
123.29
122.64
120.32
120.28
119.38
118.59
118.31
115.44
114.65
112.80
103.74
109.22
107.37
34.47
34.42
31.74
0.00
160
150
140
130
120
110
100
90
80
70
60
50
40
30
20
10
0
f1 (ppm)